HHS Public Access

Author manuscript

Ultrasound Med Biol. Author manuscript; available in PMC 2017 December 01.

Published in final edited form as:

Ultrasound Med Biol. 2016 December ; 42(12): 2743–2757. doi:10.1016/j.ultrasmedbio.2016.08.006.

Mechanisms for Induction of Pulmonary Capillary Hemorrhage by Diagnostic Ultrasound: Review and Consideration of Acoustical Radiation Surface Pressure

Douglas L. Miller

Department of Radiology, University of Michigan, Ann Arbor, MI. 48109

Abstract

Diagnostic ultrasound can induce pulmonary capillary hemorrhage (PCH) in rats and other mammals. This phenomenon represents the only clearly demonstrated biological effect of (non-contrast enhanced) diagnostic ultrasound and thus presents a uniquely important safety issue. However, the physical mechanism responsible for PCH remains uncertain more than 25 y after its discovery. Experimental research has indicated that neither heating nor acoustic cavitation, the predominant mechanisms for bioeffects of ultrasound, is responsible for PCH. Furthermore, proposed theoretical mechanisms based on gas body activation, on alveolar resonance and on impulsive generation of liquid droplets all appear unlikely to be responsible for PCH, owing to unrealistic model assumptions. Here, a simple model based on the acoustic radiation surface pressure (ARSP) at a tissue-air interface is hypothesized as the mechanism for PCH. The ARSP model seems to explain some features of PCH, including the approximate frequency independence of PCH thresholds, and the dependence of thresholds on biological factors. However, ARSP evaluated for experimental threshold conditions appear to be too weak to fully account for stress failure of pulmonary capillaries, gauging by known stresses for injurious physiological conditions. Furthermore, consideration of bulk properties of lung tissue suggests substantial transmission of ultrasound through the pleura, with reduced ARSP and potential involvement of additional mechanisms within the pulmonary interior. Although these recent findings advance our knowledge, only a full understanding of PCH mechanisms will allow development of science-based safety assurance for pulmonary ultrasound.

Keywords

Non-ionizing radiation biology; Pulmonary ultrasound; Point of Care ultrasound; Mechanical index; Lung injury mechanisms

Corresponding author: Douglas L. Miller, 3240A Medical Sciences Building I, University of Michigan Health System, 1301 Catherine Street, Ann Arbor MI 48109-5667, Tel: (734) 647-3344, FAX: (734) 764-8541, douglm@umich.edu.

Introduction

The induction of pulmonary capillary hemorrhage (PCH) by pulsed ultrasound was discovered by Child et al. (1990). A substantial literature has accumulated over more than 25 y of research on this bioeffect in various laboratory animals using pulsed ultrasound from research systems (Church and O'Brien, 2007) and from actual diagnostic ultrasound scanners (Miller et al. 2012). PCH should be expected clinically under favorable physical and biological conditions (Church et al. 2008). An example of the ultrasound images and PCH produced by 12 MHz diagnostic ultrasound is shown in Fig. 1 (Miller et al. 2015a). An interesting aspect of PCH is that induction of PCH caused by the ultrasound scanning is displayed by the ultrasound image as comet tail artifacts (CTAs), see Fig. 1. These artifacts, also called B lines, are clinically indicative for diagnosis of pulmonary edema and other conditions (Lichtenstein et al. 2009; Ahmad and Eisen, 2015). A threshold exposure response can be defined for PCH as a function of pulse pressure amplitude or intensity for a given set of exposure parameters. The studies of the threshold and magnitude of PCH have included consideration of physical parameters, such as ultrasonic frequency and pulse timing. Several mechanisms, including heating and cavitation, have been explored to explain the phenomenon, but the exact etiology remains elusive. This notable gap in our understanding of potential risks of diagnostic ultrasound represents a question of some importance, because, over this same period, the use of trans-thoracic diagnostic ultrasound for pulmonary examination has grown to be an indispensable tool in the point of care settings of emergency and intensive care (Volpicelli, 2013; Lichtenstein, 2014), as well as in traditional radiology studies. PCH appears to be the only well documented bioeffect of diagnostic ultrasound with a direct relevance to clinical pulmonary examination. Only a full understanding of PCH mechanisms will allow development of appropriate safety guidance for sonographers.

The present safety system for diagnostic ultrasound includes the detailed measurement by the manufacturer of temporal and spatial parameters of the ultrasound field generated by an ultrasound probe, including a derating attenuation factor of 0.3 dB/cm/MHz to approximate in situ tissue conditions. Two dosimetric indices are displayed on screen to aid the operator in recognizing changes in acoustical output as different settings and modes are utilized. The Thermal Index (TI) presents a reasonable worst case estimate of temperature elevation for long duration imaging with fixed position. The Mechanical Index (MI) provides a gauge of the potential worst case inception of cavitation activity by the ultrasound and indicates the derated pulse peak rarefactional pressure amplitude (PRPA) divided by the square-root of ultrasonic frequency. The primary regulated safety limitation is that the MI must be less than 1.9 MPa/MHz^{½}, which was based on the highest MI value estimated for ultrasound probes in use before May 28, 1976 (Nyborg, 2000). The TI is also generally limited to about 6 for normal approval under the 510k process of the USA Food and Drug Administration. PCH does not seem to fit this safety system, because this clearly injurious biological effect has been shown to be directly induced by diagnostic ultrasound in mammals below the regulatory limit of MI=1.9.

Here, the experimental characterization of PCH induction by clinical diagnostic ultrasound equipment and by pulse-wave simulation of diagnostic ultrasound exposure are outlined.

Five physical mechanisms, which have been proposed as hypothetical explanations for PCH, are critically reviewed. Furthermore, the mechanism of acoustical radiation surface pressure (ARSP) at a tissue-air interface is proposed as a potential explanation of PCH induced by pulsed ultrasound. The ARSP hypothesis is evaluated relative to the experimental evidence and to more complex bulk-tissue transmission parameters reported for lung. The ARSP hypothesis provides valuable insights into the phenomenon, but does not appear to fully explain the PCH bioeffect.

Experimental background

No new animal studies were performed for this research, and no human studies were reviewed. Animal studies performed for cited papers were approved by the appropriate Institutional Animal Care and Use Committee or followed ethical research guidelines of their institutions at the time of publication. The selection of papers reviewed was guided by the presence of content relevant to the mechanism for induction of PCH by diagnostic ultrasound.

The salient event for PCH is the rupture of a capillary with hemorrhage into the alveolar air space. This evolves with time into to the display of CTAs in the ultrasound image and the PCH visible on the surface of the lung and, see Fig. 1. On a microscopic level, the pulmonary structure near the visceral pleura consists of alveolar septa with broad connected air passages (Miller, 2012; Miller et al. 2014), as shown histologically in Fig. 2. The PCH fills alveoli with blood, with little indication of interstitial hemorrhage on the tissue side of the blood air barrier. PCH occurrence can be characterized by a threshold value of the ultrasonic pulse pressure amplitude in MPa or other relevant exposure metric, such as spatial peak pulse average intensity, for a specific set of experimental conditions. Recent PCH results for diagnostic ultrasound (Miller et al. 2015a) are plotted in Fig. 3. However, the dose-response trend observed is not completely deterministic (Child et al. 1990; Zachary et al. 2001; Miller 2012). That is, for apparently identical exposure conditions near the thresholds, the result for two different animals can be PCH or not (hit-or-miss), which complicates the interpretation of results. However, the threshold determinations appear to be reproducible and confirmable by different laboratories (Church and O'Brien, 2007; Miller et al. 2015b).

Research using high amplitude pulsed ultrasound from a lithotripter established that PCH effect requires gas in the lungs (Hartman et al. 1990). PCH occurred in post-natal mice with air-filled lungs at 2 MPa, but no signs of PCH were found in fetal lung, which does not contain air, even at 20 MPa. In addition, the acoustical boundary conditions at the pleural surface are important for ultrasound transmission into the lungs, which varies with the degree of inflation (O'Brien et al. 2002). For exposure to 3.1 MHz pulsed ultrasound during cessation of breathing, in situ lungs deflated to the functional residual capacity were more easily damaged than were lungs at mid-tidal volume, and lungs inflated to full tidal volume were not damaged by exposure up to 16 MPa.

PCH thresholds have been assessed for variations in pulsed ultrasound parameters (Church and O'Brien, 2007). The threshold was only weakly dependent on pulse parameters, such as

pulse duration (Child et al. 1990; O'Brien et al. 2003a). The magnitude of observed PCH depends on factors such as on-time or exposure duration. However, the possible dependence of the threshold on exposure duration is uncertain, and would indicate that the capillary rupture requires multiple pulses to accumulate susceptibility and reach failure, rather than dependence only on a single pulse amplitude, and this would be important with regard to the bioeffect mechanism. The cumulated data (Church and O'Brien, 2007) appear to be somewhat different for mice (Child et al. 1990; Raeman et al. 1993; Raeman et al. 1996; Dalecki et al. 1997; Frizzell et al. 1994), and rats (Zachary et al. 2001; O'Brien et al. 2001, O'Brien et al. 2003a; O'Brien et al. 2003b). Thresholds were about 3 MPa for rats and 0.8 MPa for mice. Interestingly, these two sets of studies had quite different exposure parameter sets: the rat data involved pulse durations mostly in the range 1.1–1.4 μs, a PRF of 1 kHz and exposure duration of 10s, while the mouse data involved a pulse duration of 10 μs, PRF of 0.1 kHz and exposure duration of 180 s. The difference in thresholds does not appear to be due to a species difference, because tests with similar exposure parameters gave similar results (Frizzell et al. 1994; Zachary et al. 2001). The duty cycle was about the same for both sets of data. Possibly, the most important difference for the threshold difference was the exposure duration difference of 10 s or 180 s. The threshold may also depend on exposure duration for diagnostic ultrasound (Miller et al. 2016a).

The ultrasonic frequency is a key parameter, and is included in the Mechanical Index as the inverse square root of pulse center frequency. For focused ultrasound, either in laboratory pulsed ultrasound systems or diagnostic ultrasound, the beam width typically decreases with frequency. The magnitude of effects depend on beam width, but the threshold apparently does not (O'Brien et al. 2001; Miller et al. 2015b). Indeed, the threshold was found to be about the same for focused or unfocused ultrasound (Child et al. 1990). In early pulsed ultrasound research on mice, the threshold was found to have a dependence on frequency similar to the MI=0.63 (American Institute of Ultrasound in Medicine, 2000a) over the range 1 – 4 MHz. In particular, the spatial peak, pulse average intensity ($\mathbf{I_{sppa}}$) threshold at 1.2 MHz and 3.7 MHz for focused ultrasound (10 μs pulses at 0.1 kHz PRF) were 11 W cm^{-2} and 40 W cm^{-2}, respectively (Child et al. 1990). However, research on rats did not reveal a clear frequency dependence (Zachary et al. 2001; O'Brien et al. 2001). Our recent study using diagnostic ultrasound showed that the magnitude of PHC induced by diagnostic ultrasound depends on frequency over the range 1.5–12 MHz (owing to the differences in beam width) (Miller et al. 2015a). Exposure response data are plotted in Fig. 3 against the spatial peak, pulse average intensity ($\boldsymbol{I_{sppa}}$). The response is apparently zero up to a threshold for the effect, and then increases rapidly for further increases in exposure level. There was little dependence of PCH thresholds on frequency as shown in Fig. 4 for rats (Miller et al. 2015a, 2015b, 2015c). This lack of significant frequency dependence for the thresholds in rats reduces the expectation that cavitation or resonance phenomena are important for induction of PCH. The in situ $\boldsymbol{I_{sppa}}$ thresholds for rats are substantially less than the intensities corresponding to the guideline upper limit of the MI (MI=1.9), Fig 4, although the comparison depends on assumptions about attenuation across the intercostal space (i. e. the MI parameter includes a relatively low attenuation).

Biological or physiological factors appear to be as important in some cases as pulse pressure amplitudes and other physical exposure conditions. Different mammalian species appear to have about the same threshold range for mice, rats and pigs (American Institute of Ultrasound in Medicine, 2000a; Church et al. 2008). However, the age of the subject has also been evaluated as a risk factor, with an indication of increased sensitivity with age (Dalecki et al. 1997; O'brien et al. 2003b). For ultrasound exposure, laboratory animals typically have been anesthetized by ketamine plus xylazine. Recently, we found that PCH induction was strongly influenced by anesthesia methods in rats. Specifically, the use of the veterinary sedative xylazine (Miller et al. 2015c) or the related clinical sedative dexmedetomidine (Miller et al. 2016b) significantly lowered the ultrasound threshold for PCH relative to use of ketamine only. A threshold determined using ketamine only is plotted in Fig. 4. This dependence on physiological factors seems to be an important consideration for understanding the etiology and physical mechanism of ultrasound induced PCH. If subtle physiological differences in the test subjects are important, then the puzzling hit-or-miss nature of the results noted above may be explained by subtle physiological differences between individual rats.

Theoretical background

The present collection of experimental research findings contains sufficient information to support critical evaluation of various potential physical mechanisms for ultrasound induced PCH. Here, five prospective mechanisms are considered: heating, cavitation, gas-body activation, alveolar resonance, and impulsive liquid jetting.

Heating

Heating of fragile lung tissue hypothetically might be important even for low time-average intensity pulsed ultrasound due to the potentially high absorption coefficient of lung tissue and the insulating factor of the gas. However, the expected heating effect of diagnostic ultrasound appears insufficient to explain the ultrasonic PCH effect. No thermal injury is expected for elevations less than 2 °C even for hou rs-long durations, and the TI for diagnostic ultrasound typically is less than 1 for B mode scanning. The lung does not appear to be selectively heated by ultrasound, relative to other tissues, and is cooled by blood and air flows. The temperature elevation produced at the surface of mouse lung was approximately 1 °C after 5 min of 4.2 MHz unfocused ultrasound exposure by a 1 W/cm^2 continuous wave with heating equivalent to relatively high intensity pulsed ultrasound (Hartman et al. 1992). Furthermore, thermal lung injury from an infrared laser was found to produce thermal coagulation of lung tissue and fluid, which was quite unlike alveolar hemorrhage produced by pulsed ultrasound (Zachary et al. 2006).

Ultrasonic cavitation

A well-known mechanism for nonthermal bioeffects is ultrasonic cavitation, which was initially thought to be the likely cause of PCH. Holland et al. (1996) reported direct evidence from an active cavitation detector for cavitation from diagnostic ultrasound exposure in rats in association with PCH. Also, as noted above, early findings for PCH appeared to display a threshold frequency dependence similar to that of the Mechanical Index, which was created

as a guide for potential cavitational bioeffects (American Institute of Ultrasound in Medicine, 2000a). However, later research indicated that cavitation was not involved in ultrasonic PCH. Positive and negative pulses did not show the PRPA to be a key parameter, as would be expected for a purely cavitational mechanism (Bailey et al. 1996; Frizzell et al. 2003). A classic test for cavitational effects is inhibition by static overpressure. O'Brien et al. (2000) showed that an overpressure of 1 MPa did not suppress the PCH effect, relative to atmospheric pressure, from 2.8 MHz pulsed ultrasound over the range from 2.8 to 11.8 MPa, but rather actually appeared to increase the severity of PCH. Another test for involvement of cavitation in bioeffects is to modify the population of cavitation nuclei, which is normally quite low in vivo. The injection of microbubble ultrasound contrast agents, which can serve as cavitation nuclei, did not increase the sensitivity to PCH for 1.1 MHz (Raeman et al. 1997) or 3.1 MHz pulsed ultrasound (O'Brien et al. 2004). Indeed, the pressure amplitude is actually reduced at the lung surface, and relatively low in the interior of the lung, due to the reflection from the tissue-air interface. This low PRPA environment probably accounts for the lack of enhancement with injected contrast agents and implies minimal cavitational activity. The explanation of the apparently different frequency dependence found in early work on mice, which supported the cavitation hypothesis, is uncertain. Subsequent research by Zachary et al. (2001) showed no statistical difference for PCH between 2.8 MHz and 5.6 MHz ultrasound nor between mice and rats. As noted below, however, cavitation or gas body activation may have a secondary role in the lung injury.

Gas body activation

Another mechanism associated with the presence of gas in tissue is gas body activation (Nyborg et al. 2002). Gas body activation can occur when stable bodies of gas interact with ultrasound fields. In biological media with gas bodies, such as insect larvae and plant roots, the gas body activation results in structural oscillation and even resonance with cell disruption by acoustic microstreaming, depending on the ultrasound exposure (Miller, 1987). The structure of mammalian lung tissue hypothetically seems to have some features suitable for gas body activation: branching gas-filled bronchioles end in alveolar sacs (Levitzky, 2013). Some anatomical illustrations appear to show clusters of spherical alveolar "bubbles", and modeling of lung as collection of 300 μm spherical gas bubbles in a liquid-like medium was utilized in early considerations of the high attenuation coefficient of lung tissue (Dunn and Fry, 1961). However, the bubble model is not a realistic representation of the pulmonary structure. One alveolar septum, which is only a few microns thick in many areas, has gas on both sides. Within the volume of air, the alveolar sacs at the terminus of the tracheobronchial tree have delicate alveolar septa containing large numbers of capillaries arranged in a net-like morphology (Levitzky, 2013). Histological preparations of rat lung tissue, as in Fig. 2, show the preponderance of gas space and alveolar sacs completely open to the alveolar ducts and bronchioles. That is, there is no physically definable alveolar gas body and therefore, alveolar gas body activation does not seem to help explain the initial (threshold) event for PCH.

Gas body activation may have a secondary role in PCH development after initiation. As noted in the Introduction, the pristine lung surface is seen as a bright line of echoes with only reverberation artifacts displayed beyond the pleural surface (Fig. 1). After capillary

hemorrhage (Fig. 1), the alveolus appears to flood as the surface tension rises and approximately spherical bubbles can form. A close up image of a PCH area in rat lung about 10 min after scanning presented in Figure 5 shows residual gas bubbles < 100 μm diameter within the PCH scan area. These large bubbles scatter ultrasound very well and result in comet tail artifacts in the ultrasound images (Fig. 1). In some sense, this process could be considered to be gas body activation. Interestingly, all the other gas volumes within the hemorrhage volume (Fig. 5) have broken up or dissolved. The process of flooding, bubble formation and dissolution could potentially result in some cavitation activity by nucleation from the disappearing gas bubbles. The gas body activation would be distinct from the initial PCH occurrence, but might aid in the progression of the hemorrhage region with depth into the lung.

Alveolar resonance

An alveolar resonance mechanism has been proposed by Jabaraj and Jaafar (2012, 2013a, 2013b). The alveolar septa were modeled as elastic circular membranes, vibrating in a fundamental resonance mode. Resonance is a mechanism by which energy can build in a vibrating structure, possibly reaching damaging amplitude. The strain in the model membrane was determined and an injurious level was calculated based on plasma membrane stress failure in alveolar epithelial cells. The results indicated a strong increase in thresholds for injury with frequency, with no injury for frequencies greater than 1.55 MHz when the MI was less than 1.9, as expected for diagnostic ultrasound (Jabaraj and Jaafar, 2013b). However, the physical model appears to be an unrealistic description of lung tissue in several ways. The alveolar wall at the lung surface subjected to ultrasound pulses is not a free circular membrane, but rather it forms the complex structure of the visceral pleura (American Institute of Ultrasound in Medicine. Section 3, 2000b; Levitzky, 2013). In addition, the septa are not simple membranes, as revealed by scanning electron microscopy, but contain a complex network of capillaries (Kuhn and Finke, 1972; Alexander et al. 1973; Kendall and Eissmann, 1980; Schraufnagel et al. 1986; Caduff et al. 1986). An example of a corrosion cast of pulmonary capillaries is shown in Fig. 6. The septa in the interior of the lung would not be subjected to forcing, because the ultrasound pressure would be the same on both sides of the septa which essentially share the common air space (Levitzky, 2013). The septa are not stretched like a drumhead, but rather are flaccid, subject to surface tension (Bachofen and Wilson, 1997). The postulated resonance also does not seem to take into account the brief duration of pulsed ultrasound (1–3 cycles in B mode pulse-echo) for which resonant accumulation of energy would be minimal. Finally, the calculated ultrasonic pressure thresholds increase strongly with frequency, in contrast to the minimal frequency dependence found experimentally for diagnostic ultrasound (Miller et al. 2015a). The proposed alveolar resonance mechanism (Jabaraj and Jaafar, 2012, 2013a, 2013b) does not appear to explain the PCH bioeffect of diagnostic ultrasound.

Impulsive liquid jetting

Finally, a mechanism for PCH involving the impulsive generation of liquid drops by focused ultrasound has been proposed by Tjan and Phillips (2007, 2008). When focused ultrasound is directed upward at a water-air interface, the acoustical radiation pressure on the surface can induce the formation of a “fountain” for high intensity tone bursts. This mechanism is

quite a potent bioeffect mechanism for high intensity focused ultrasound when the fountain originates at the surface of tissue and emulsifies the tissue into droplets (Simon et al. 2012). The fountain effect has several interesting features including the jet, with a diameter comparable to the beam diameter, and rapid production of small droplets (sometimes producing acoustical “fog”). Under some conditions, single droplets can be generated at the tip of the fountain and expelled upward. This phenomenon can occur for small size scales, for which surface tension is important, and has been studied for possible application to inkjet printing (Elrod et al, 1989). The model for PCH envisaged pulsed ultrasound incident on a free water-air interface, from which droplets are expelled that puncture the alveolar sacs, causing them to fill with blood (Tjan and Phillips, 2007). Droplet ejection is expected to occur for a critical value of the Weber number, a dimensionless number relating to the relative importance of fluid inertia and surface tension. The critical conditions were associated with the ultrasonic Mechanical Index and predicted droplet ejection for MI ≥ 0.5, in approximate agreement with early experimental findings of PCH (Tjan and Phillips, 2007). However, impulsive liquid jetting seems to be an unlikely mechanism for diagnostic ultrasound induced PCH for several reasons. As noted above, the dependence of ultrasound induced PCH on frequency has since been found to be weaker than that of the MI (Miller et al. 2015a). More importantly, however, the model is difficult to reconcile with actual pulmonary structures. There is no free water interface available to launch droplets at the lung surface; the structure consists of the chest wall, thin parietal and visceral pleura membranes and the alveolar sacs containing air (Levitzky, 2013). The surfactant layer within the alveoli is minimal, and reduces the surface tension to a few mN/m (compared to 56 mN/m for blood). The alveolar structures have tissue properties and capillaries, as well as surface tension. These only approach the ideal water air interface at the blood air barrier of capillaries, which are much smaller than the beam-width size of the jetting mechanism. Although the calculations based on the impulsive liquid jetting model of Tjan and Phillips (2007) are noteworthy, key features of the model are difficult to reconcile with actual biophysical conditions at the pleural capillaries and so this model too does not appear to explain the PCH bioeffect of diagnostic ultrasound.

Consideration of ultrasound interaction with the blood-gas barrier

The steady forces and pressures generated by the propagation of an ultrasound beam can serve as mechanisms for bioeffects of ultrasound. These are second order quantities (as opposed to the first order oscillatory pressure, displacement and velocity) associated with the intensity and energy carried by the wave (Nyborg, 1978). The acoustical radiation force or pressure has several important applications to medical ultrasound (Nyborg et al. 2002; Duck, 2008; Sarvazyan et al, 2010). For an absorbing medium, a body force is generated throughout the beam which can cause tissue displacement or fluid flow. The tissue displacement phenomenon recently has been exploited for the acoustical radiation force impulse (ARFI) mode of diagnostic ultrasound elastography (Shiina et al. 2015). A relatively simple situation is the pressure generated by an ultrasound wave directed perpendicularly upon a surface separating two media of different acoustic impedance. The direction and magnitude of this pressure depends on the relative impedances of the two media incident intensity (Beyer, 1997). For a beam direct upward at an air-water interface,

the beam is essentially reflected back on itself, and the upward deflection of the liquid surface by the radiation pressure can include vigorous perturbation, such as the acoustic fountain effect noted above for sufficient ultrasound intensities (see *Impulsive liquid jetting*). The potential of this phenomenon to be a mechanism for bioeffects of diagnostic ultrasound is modest, but bioeffects appear to include generation of tactile sensations, cardiac responses, and possible fetal startle reactions (ECMUS, 2000; Nyborg et al. 2002; Duck, 2008).

Acoustical radiation surface pressure (ARSP) as the PCH mechanism

The ultrasound transmitted to lung passes through the chest wall, normally at an intercostal space, and interacts with the visceral pleura. The alveolar wall at the visceral pleura consists for the most part of several thin cell layers, a complex meshwork of pulmonary capillaries and the air-filled alveoli. Ultrasound pulses interact with the pleural surface, which may be modeled approximately, at the scale of the alveolus, as a simple tissue-air interface. This ARSP model assumes perfect reflection at the interface owing to the large differential in acoustical impedance (intensity transmission is only 0.1% for atmospheric pressure at a water-air interface). The reflection produces a steady state (i. e. without acoustical cyclic variation) radiation surface pressure $\boldsymbol{P_{RSa}}$ at the tissue-air barrier given by

$$P_{RSa}=\frac{2I_i}{c_{tis}}, \quad (1)$$

in which $\boldsymbol{I_i}$ is the incident ultrasonic intensity and $\boldsymbol{c_{tis}}$ is the speed of sound in the tissue (Nyborg, 1978; Duck, 1998; Wang and Lee, 1998). $\boldsymbol{P_{RSa}}$ is a second order quantity which is positive toward the air side in this case. It is important to realize that the first-order pressure amplitude is theoretically identical on both sides of the barrier and therefore produces no excess stress.

The incident intensity of a pulsed ultrasound beam relevant to the bioeffect is the peak pulse (as measured for the PRPA) aimed directly at the lung as the beam sweeps across the surface, which can be expressed as the spatial-peak, temporal-average ($\boldsymbol{I_{spta}}$) or the spatial-peak pulse-average ($\boldsymbol{I_{sppa}}$) values. For B mode ultrasound, the temporal average includes duty cycle timing of the pulse duration, the pulse-repetition frequency (PRF), and the frame rate. The different pulse timing regimes are illustrated in Fig. 7. The pulse repetition frequency has a duty cycle of 0.032, and the frame rate adds an approximate duty cycle of 0.04, giving a temporal averaging reduction of roughly 1,000:1 from $\boldsymbol{I_{sppa}}$ to $\boldsymbol{I_{spta}}$. Using $\boldsymbol{I_{spta}}$, the average of $\boldsymbol{P_{RSa}}$ over the pulse and image repetition frequencies would be insignificant relative to even the capillary blood pressure at thresholds for PCH. However, the values of $\boldsymbol{P_{RSa}}$ for $\boldsymbol{I_{sppa}}$ may be comparable to capillary blood pressures and add to the blood pressure-generated capillary wall stresses. Both the peak rarefactional and peak compressional amplitudes seem important and $\boldsymbol{I_{sppa}}$ appears to be a good exposure parameter for PCH (Bailey et al. 1996; Frizzell et al. 2003). Our previous studies of PCH in rats provided data for thresholds in terms of the in situ $\boldsymbol{I_{sppa}}$, which are listed in Table 1. $\boldsymbol{P_{RSa}}$ values during the pulses calculated from Eq. 1 are also presented in Table 1 (for

comparisons of pressure units, 1 Pa equals 0.01 cmH_2O or 0.0075 mmHg). The calculated threshold values of $\boldsymbol{P_{RSa}}$ were modest, averaging about 290 Pa for fixed beam pulse-wave exposure, and 586 Pa for B mode. For B mode, the threshold $\boldsymbol{P_{RSa}}$ was higher at 1900 Pa when ketamine alone or isoflurane was used for anesthesia. The $\boldsymbol{P_{RSa}}$ for the maximal level of diagnostic ultrasound of 300 W cm^{-2} at 4.5 MHz (Fig. 3) was 4 kPa (30 mm Hg).

There have been several other studies of PCH with thresholds determined in rats (Church and O'Brien, 2007), but these were reported in terms of the peak rarefactional pressure amplitude or estimated MI, and the threshold $\boldsymbol{I_{sppa}}$ is not clearly available from the publications. The PRPA values were generally not greatly different for these reports from those shown in Table 1, indicating that the $\boldsymbol{I_{sppa}}$ would be similar to the values reported here. However, several studies using relatively short duration exposures found somewhat higher thresholds (O'Brien et al. 2001; O'Brien et al. (2003a). O'Brien et al. (2001) used 2.8 MHz (1.42 μs pulses) and 5.6 MHz (1.14 μs pulses) and found occurrence PRPA thresholds of 2.3 MPa and 2.8 MPa, respectively. The $\boldsymbol{I_{sppa}}$ can be estimated from the PRPAs to be about 176 W cm^{-2} and 261 W cm^{-2}, which give calculated $\boldsymbol{P_{RSa}}$ results of 2340 Pa (17.6 mmHg) and 3470 Pa (26 mmHg) at 2.8 and 5.6 MHz, respectively. O'Brien et al. (2003a) used 2.8 MHz ultrasound with 1.3, 4.4, 8.2 and 11.6 μs pulses found occurrence PRPA thresholds of 3.1, 2.8, 2.3, and 2.0 MPa, respectively. The corresponding estimated $\boldsymbol{I_{sppa}}$ threshold are 320, 261, 176, and 133 W cm^{-2}, which give calculated $\boldsymbol{P_{RSa}}$ results of 4260, 3470, 2340 and 1770 Pa (32, 26, 18 and 13 mmHg), respectively.

The early results from mice are of interest because they indicated significant frequency dependence of the threshold. Values of in situ $\boldsymbol{I_{sppa}}$ were provided by Child et al. (1990) for 3 min pulsed-wave (fixed beam) exposures, and included 11 Wcm^{-2} for 1.2 MHz ultrasound and 40 Wcm^{-2} for 3.7 MHz ultrasound both pulsed at 10:10000 μs. These intensities yield $\boldsymbol{P_{RSa}}$ values of only 133 Pa and 532 Pa (1 mmHg and 4 mmHg), respectively, for the mouse study, which are somewhat less or greater than comparable values for rats (Table 1). As noted above, the reason for the different frequency dependence seen in this early work on mice and later research is uncertain.

Assessment of the ARSP model relative to pulmonary physiological parameters

The pulmonary capillaries are configured to maximize gas exchange between the blood and alveolar air. The blood air barrier is 0.2–0.3 μm thick but extends over 50–100 m^2 (West, 2000). This thin interface includes elements of the alveolar epithelium, basement membrane and capillary endothelium. Subpleural capillary diameters in rats are reported to be 6.6 ± 1.6 μm (Short et al. 1996). The right side blood pressure is substantially less than in the left side of the circulation: pulmonary artery and capillary blood pressures are 15 mmHg (20 cmH_2O) and 8–12 mmHg (11–16 cmH_2O), respectively (Levitzky, 2013). The pulmonary circulation passively accommodates the wide range of circulating blood volumes ranging from those occurring in sleep to those in vigorous excise by recruitment and distension of the capillary bed. When full of blood the capillaries can be approximately cylindrical and bulge into the air space from the alveolar surfaces. The capillaries have complex morphology, as shown in electron microscopy, see Fig. 6 (Kuhn and Finke, 1972; Alexander et al. 1973; Kendall and Eissmann, 1980; Schraufnagel et al. 1986; Caduff et al. 1986). The structures and stresses in

a pulmonary capillary are illustrated in Fig. 8 (West and Mathiew-Costello, 1999; West, 2000). In the simple ARSP model, the ultrasonic $\boldsymbol{P_{RSa}}$ adds to the blood pressure on the inside of the blood-air barrier, and adds to stress in the capillary wall, thereby potentially leading to PCH.

Although the pulmonary circulation is capable of great accommodation of fluctuating blood flow by recruitment and distention of capillaries, the accommodation takes some time. There is little data on this timing, but the compliance response may take ~0.4 s, as determined for frog mesentery (Swayne and Smaje, 1989). For capillaries already at full stress due to physiological conditions, the microcirculation likely could not respond to and accommodate the extra stress during the brief $\boldsymbol{P_{RSa}}$ impulse. This could occur in local regions, exceeding the capillary rupture strength. This hypothesis implies that microscale variations in capillary conditions might impart some characteristics of stochastic phenomenon to the induction of PCH, and could help to explain the hit-or-miss nature of PCH for animals scanned with seemingly identical near-threshold conditions.

The stressing pressure needed to injure pulmonary capillaries has been studied in reference to several physiological conditions (West and Mathiew-Costello, 1999; West, 2013). Stresses in the pulmonary capillary are illustrated in Fig. 8. The pressure appears to be supported by a thin layer, possibly only 50 nm thick, of type IV collagen in the blood gas barrier as illustrated in Fig. 9 (West and Mathiew-Costello, 1999; West, 2000). Testing in perfused rabbit lungs has indicated stress failures at about 39 mmHg transmural pressure and some changes at about 22 mmHg (West et al. 1991). Pulmonary capillary pressures can exceed 30 mmHg during exercise (West and Mathiew-Costello, 1992a). This type of stress can lead to capillary rupture for extreme exercise, such as in race horses (West, 2013), or in high altitude pulmonary edema (West and Mathieu-Costello, 1992b; Maggiorini et al, 2001). Newborns appear particularly susceptible (Fu et al. 2003). Other conditions leading to increased pressure-stress in the pulmonary circulation, such as pulmonary hypertension and left ventricular heart failure can also lead to capillary compromise and pulmonary edema (West, 2013). Therefore, not uncommon physiological conditions appear to overlap with conditions sufficient for stress failure of capillaries and may prime the capillaries to ultrasound induced PCH.

The ARSP mechanism appears to be supported by several features of observations of PCH. Since $\boldsymbol{P_{RSa}}$ depends on ultrasonic intensity, it is essentially independent of the ultrasound frequency, a feature which has been observed for PCH (Miller et al. 2015a). The PCH from $\boldsymbol{P_{RSa}}$ should add to stress present due to various physiological conditions. For example, the anesthetic components xylazine and dexmedetomidine, α_2 adrenergic receptor agonists which effect pulmonary circulation, have a strong enhancing influence on PCH (Miller et al. 2015c; Miller et al. 2016a). Xylazine is a sedative and analgesic which produces significant cardiovascular and respiratory depression (Flecknel, 2009). Xylazine has been reported to induce pulmonary edema in rats with relatively high doses of 21–45 mg/kg (Amouzadeh et al 1991; 1993). Capillaries stressed by physiological conditions sufficient to produce edema may be quite sensitive to even small impacts from ARSP.

Maximal B-mode ultrasound pulses may achieve ARSP substantially greater than normal capillary blood pressures with a potential for injury. However, the magnitude of the P_{RSa} for some near-threshold conditions seems too small to be important. If the pulmonary capillary blood pressure is in the high normal range, about 15 mmHg, then added stress of 7 to 24 mmHg may be needed to injure the blood-gas barrier. Higher than normal physiological pressures, which can reach 30 mmHg or more, may require less added stress for injury. The P_{RSa} associated with thresholds for short duration exposure noted above may reach these levels, but P_{RSa} thresholds for B mode ultrasound scanning (with xylazine) averaged a modest 4.4 mmHg. P_{RSa} thresholds for pulse wave exposure in rats averaged only 2.1 mmHg (see Table 1) and possibly as low as 1 mmHg in mice. Edema may occur at a lower level of perturbation than PCH, involving only a separation of the epithelial and endothelial cells (West and Mathiew-Costello, 1999). PCH represents greater injury with breach of all 3 layers of the blood air barrier (Fig. 8), which may require higher stresses than those responsible for edema. Edematous injury seemed to be rapidly reversible (West and Mathiew-Costello, 1999) but the capillary rupture injury may not be rapidly reversible, leading quickly to the observable PCH. Research is needed to explore factors which could amplify the impact of small pulse P_{RSa} values, such as accumulation of strain, collagen matrix distortions from repeated pulses, or membrane fatigue and failure with time for longer duration exposures. In addition, the simple ARSP model should be elaborated to help understand PCH occurring after the initial surface effect, when the PCH can continue growing in depth and fill the entire thickness of a lobe (Miller et al. 2016b). Examination of P_{RSa} or related frequency independent mechanisms seem to be a promising approach in the search for the explanation PCH induced by diagnostic ultrasound.

Consideration of bulk properties and transmission of ultrasound into the lung

Important tissue parameters for biomedical ultrasound include the density ρ_{tis}, speed of sound c_{tis} and attenuation or absorption. These enable calculation of ultrasound reflection and transmission at boundaries from the tissue acoustical impedance $z_{tis}=\rho_{tis}c_{tis}$. Lung parameters are quite different from those of solid tissues such as heart, liver and kidney. In consideration of surface radiation pressure P_{RSa} above, the pleural surface was modeled as a tissue-air boundary, approximately the case microscopically for the blood-air barrier. The low density of air (ρ_{air} = 1.2 kg m^{-3}, compared to soft tissues, ρ_{tis} = 1050 kg m^{-3}) leads to nearly perfect reflection. If the lung organ is considered in bulk, however, tissue parameters can be measured similarly to other tissues. The bulk density of lung ρ_{lung} is about 200 – 400 kg m^{-3} for about 80–60 % air, depending on inflation and position (El-Khatib et al. 1989; Hopkins et al. 2007). By visual inspection of histological samples (e. g. Fig. 2) the density at the pleural surface with no large blood vessels appears to be lower, perhaps 100 kg m^{-3}, with about 90 % air and 10 % alveolar septa. However, on a larger scale, it seems reasonable to model the lung using the bulk properties.

The speed of sound and attenuation of lung were investigated by Dunn and Fry (1961) and Dunn (1974; 1986). The speed of sound c_{lung} was found to increase with frequency from 658 m/s at 1 MHz to 1180 m/s at 5 MHz; for comparison, soft tissues have approximately c_{tis} = 1550 m/s and air has c_{air} = 353 m/s at body temperature. Values for 1–7 MHz from Dunn (1986) are plotted in Fig. 10. The attenuation was relatively high and increased rapidly

with frequency from 37.3 dB/cm at 1 MHz to 101 dB/cm at 5 MHz, whereas soft tissues have typical attenuation of about 0.5 dB/cm-MHz. O'Brien et al (2000) tested 2.8 MHz ultrasound exposure for the cavitation mechanism my applying external hydrostatic pressure. For atmospheric pressure, the density and speed of sound were estimated to be 414 kg m^{-3} and 812 m/s, respectively, which gives an impedance z_{lung} = 336 krayl. This value, relative to the tissue impedance of z_{tis} = 1,628 krayl, suggests that a large fraction, 41%, of the ultrasonic intensity is transmitted into the lung (O'Brien et al 2000). This important result for the bulk tissue model is quite different from the assumption of near-total reflection at the blood-air barrier. This factor was investigated for different levels of in situ lung inflation with 3.1 MHz pulse-wave exposure (O'Brien et al. 2002). For deflated lungs, substantial PCH was observed. PCH was reduced for partial inflation and eliminated for fully inflated lungs. The intensity transmitted into the lung was modeled for a range of volume fractions of air in the lungs: transmission was reduced for a high air fraction (inflation), and increased for lower air fraction (lung deflation). The observations indicate an import role for the transmitted ultrasound in PCH: increased transmission gives increase effect. Oelze et al. (2003) examined the impedance and reflection problem for ex-vivo rat lungs with varying inflation from deflated to 7, 10 and 15 cm H_2O inflation and 3.5 –10 MHz frequency. The impedance was found to be near that of water for deflated lung declining to 200 krayl for fully inflated lungs. Tests with lungs from rats, rabbits and pigs of various ages gave similar results (Oelze et al. 2008).

A bulk tissue model of the ARSP P_{RSb}, including the influence of variations in reflection and transmission, can be calculated using the formulation of Wang and Lee (1998). Using the ratio of tissue to lung impedance $Z = z_{tis}/z_{lung}$, P_{RSb} at the interface is given by

$$P_{RSb} = P_{RSa}\frac{1+Z^2-2nZ}{(1+Z)^2}, \quad (2)$$

in which $n = c_{tis}/c_{lung}$. For large $Z \gg 1$, which occurs for a tissue-air interface, P_{RSb} reduces to P_{RSa} (Eq. 1). For $Z = n = 1$, there is no impedance change, and $P_{RSb} = 0$. Calculations using Eq. 2 require information on both ρ_{lung} and c_{lung}, which are not readily available solely by measurement of reflection coefficients. Data on ρ_{lung} and c_{lung} were given for 1–7 MHz by Dunn (1986). Table 2 and Fig. 11 present values calculated for P_{RSb}/P_{RSa} using data from Dunn (1986) and also interpolated or extrapolated values at 1.5, 4.5 and 7.5 MHz for comparison to Table 1. The ARSP for the bulk model is reduced to about 20 % of that for the tissue-air model. The intensity transmission coefficient given by $4Z/(1+Z)^2$ is also shown, and increases from 47% to 80% from 1–7 MHz. However, the attenuation within the lung is high relative to soft tissue, as noted above, and the transmitted intensity would rapidly decline with depth through scattering or absorption. For the 100 dB/cm attenuation given for 5 MHz (Dunn, 1986), the intensity would be reduced by half (−3 dB) for a depth of only 300 μm.

These considerations imply that the transmission of ultrasonic energy into the lungs introduces a potential for effective interaction on the gas side of the blood-air barrier. This

model may also aid in understanding the progression of the PCH into the lung lobes after initiation at the surface. Operative mechanisms for PCH may act inside the lung as well as on the pleural surface. The observation that the increased hydrostatic air pressure used to test for cavitation actually increased the PCH effect further supports this concept (O'Brien et al. 2000). Nevertheless, the key physical feature of lung is its extreme heterogeneity, and the simple bulk model is difficult to reconcile with the heterogeneous structure of lung. On a microscopic scale (Fig. 2), transmission of 47–80 % of the ultrasound into the lung is a difficult concept. At a threshold of 1 MPa, 50% transmission implies pressure amplitudes of 500 kPa inside the lung. However, this is physically impossible to achieve in the air spaces, because it requires a negative tension of 400 kPa (500 kPa minus 100 kPa atmospheric pressure), which cannot be supported by the gas. Transmitted ultrasound must strongly perturb the alveolar septa, and this heterogeneous transmission would surely create strong perturbation of the blood – air barrier. Local ARSP may range from $\boldsymbol{P_{RSa}}$ to $\boldsymbol{P_{RSb}}$ giving a heterogeneous impact on the pulmonary surface. Detailed modeling will be needed to explore these phenomena and reconcile the microscopic interaction with the macroscopic bulk properties.

Conclusion

Diagnostic ultrasound can induce pulmonary capillary hemorrhage (PCH) in rats and other mammals. This phenomenon represents a complex clinical safety issue as well as a scientific puzzle. The physical mechanism responsible for PCH remains uncertain more than 25 y after its discovery. PCH occurs above thresholds in the exposure levels, which may be specified in terms of pulse average intensity or pressure amplitudes. Recent work has indicated little dependence of thresholds on ultrasound frequency. In addition, physiological conditions, such as changes induced by different anesthesia methods, play an important role in the sensitivity of lung to ultrasound.

Six mechanisms have been explored to explain the induction of PCH by ultrasound. Experimental research has indicated that heating is too low for diagnostic ultrasound (or pulsed wave ultrasound used to simulate diagnostic exposure) to cause thermal injury. Acoustic cavitation, the major bioeffect mechanism for contrast-enhanced ultrasound, has been shown not to be the causative factor for PCH, even with gas-body contrast agents in the circulation. Furthermore, proposed theoretical mechanisms based on pulmonary modeling involving gas body activation of alveolar gas, alveolar resonance of the septa and impulsive generation of liquid droplets all appear unlikely to be responsible for PCH, due to unrealistic features assumed for the lung in each of the models.

Here, a simple model based on the acoustic radiation surface pressure (ARSP) at a tissue-air interface is hypothesized as a potential mechanism for PCH. Ultrasound is almost completely reflected by a tissue air interface, which creates a positive pressure impulse on the interface toward the air. This pressure would add to the pressure differential across the blood-air barrier. ARSP is directly proportional to the ultrasound intensity and easily calculated from the spatial peak pulse average intensity (Eq. 1). The ARSP model seems to explain some features of PCH, including the approximate frequency independence of PCH thresholds, and the dependence of thresholds on biological factors which can affect

pulmonary capillary circulation. For some threshold conditions, the ARSP appears to be comparable to pulmonary capillary blood pressures. Stressful physiological conditions commonly occur and overlap with levels of physiological stress which can injure pulmonary capillaries and induce edema or PCH. Therefore, small additional physical stresses from the impact of ultrasound pulsed might be capable of inducing PCH in pre-stressed capillaries before the circulation can adjust to the change. However, ARSP evaluated for the lowest threshold conditions appears to be too small to fully account for PCH. Furthermore, consideration of bulk properties of lung tissue suggests substantial transmission of ultrasound through the pleura, with reduced average ARSP and potential involvement of additional mechanisms within the pulmonary interior.

This review indicates substantial advances toward the mechanisms and etiology of PCH, but further research is needed to resolve uncertainties. Future research is needed to better delineate the physiological conditions which sensitize lung to PCH and to help identify at risk patients. Data is also needed on the microscopic details of capillary failure and on the progression of PCH with time to help gauge the potential clinical impact of PCH. Improved theoretical models of the interaction of ultrasound pulses with lung, for example, using detailed finite amplitude methods, are needed to fully describe the PCH phenomenon at the capillary level. An improved understanding of the mechanisms and processes involved in PCH will allow for science-based development of appropriate safety assurance for pulmonary diagnostic ultrasound.

Acknowledgments

Research reported in this publication was supported by the National Heart Lung and Blood Institute of the National Institutes of Health under award number R01HL116434. The content is solely the responsibility of the author and does not necessarily represent the official views of the National Institutes of Health.

References

Ahmad, S.; Eisen, LA. Lung ultrasound: the basics. In: Lumb, P.; Karakitsos, D., editors. Critical care ultrasound. Vol. Ch 19. Philadelphia: Elsevier; 2015. p. 106-110.

Alexander IG, Ritchie BC, Maloney JE. Scanning electron microscopy of pulmonary alveolar capillary vessels. Thorax. 1973; 28:222–227. [PubMed: 4731118]

American Institute of Ultrasound in Medicine. Section 4--bioeffects in tissues with gas bodies. J Ultrasound Med. 2000a; 19:97–108. 154–68. [PubMed: 10680616]

American Institute of Ultrasound in Medicine. Section 3--selected biological properties of tissues: potential determinants of susceptibility to ultrasound-induced bioeffects. J Ultrasound Med. 2000b; 19:85–96. 154–68. [PubMed: 10680615]

Amouzadeh HR, Sangiah S, Qualls CW Jr, Cowell RL, Mauromoustakos A. Xylazine-induced pulmonary edema in rats. Toxicol Appl Pharmacol. 1991; 108:417–27. [PubMed: 1902333]

Amouzadeh HR, Qualls CW Jr, Wyckoff JH 3rd, Dzata GK, Sangiah S, Mauromoustakos A, Stein LE. Biochemical and morphological alterations in xylazine-induced pulmonary edema. Toxicol Pathol. 1993; 21:562–71. [PubMed: 8052803]

Bachofen, H.; Wilson, TA. Micromechanics of the acinus and alveolar walls. In: Crystal, RG.; West, JB.; Barnes, PJ.; Weibel, ER., editors. The Lung: Scientific foundations. 2. Philadelphia: Lippincott-Raven Publishers; 1997. p. 1159-1167.

Bailey MR, Dalecki D, Child SZ, Raeman CH, Penney DP, Blackstock DT, Carstensen EL. Bioeffects of positive and negative acoustic pressure s in vivo. J Acoust Soc Am. 1996; 100:3941–3946. [PubMed: 8969491]

Beyer, RT. Nonlinear Acoustics. College Park, MD: American Institute of Physics; 1997.

Caduff JH, Fischer LC, Burri PH. Scanning electron microscope study of the developing microvasculature in the postnatal rat lung. Anat Rec. 1986; 216:154–164. [PubMed: 3777448]

Child SZ, Hartman CL, Schery LA, Carstensen EL. Lung damage from exposure to pulsed ultrasound. Ultrasound Med Biol. 1990; 16:817–825. [PubMed: 2095012]

Church CC1, O'Brien WD Jr. Evaluation of the threshold for lung hemorrhage by diagnostic ultrasound and a proposed new safety index. Ultrasound Med Biol. 2007; 33:810–818. [PubMed: 17383801]

Church CC, Carstensen EL, Nyborg WL, Carson PL, Frizzell LA, Bailey MR. The risk of exposure to diagnostic ultrasound in postnatal subjects: nonthermal mechanisms. J Ultrasound Med. 2008; 27:565–592. [PubMed: 18359909]

Dale PJ, Matthews FL, Schroter RC. Finite element analysis of lung alveolus. J Biomech. 1980; 13:865–73. [PubMed: 7462260]

Dalecki D, Child SZ, Raeman CH, Cox C, Penney DP, Carstensen EL. Age dependence of ultrasonically induced lung hemorrhage in mice. Ultrasound Med Biol. 1997; 23:767–776. [PubMed: 9253825]

Duck, FA. Radiation pressure and acoustic streaming. In: Duck, FA.; Baker, AC.; Starritt, HC., editors. Ultrasound in Medicine. Vol. Chap 3. Institute of Physics Publishing; Bristol; UK: 1998. p. 39-56.

Dunn F, Fry WJ. Ultrasonic absorption and reflection by lung tissue. Phys Med Biol. 1961; 5:401–410. [PubMed: 13725043]

Dunn F. Attenuation and speed of ultrasound in lung. J Acoust Soc Am. 1974; 56:1638–1639. [PubMed: 4427035]

Dunn F. Attenuation and speed of ultrasound in lung: dependence upon frequency and inflation. J Acoust Soc Am. 1986; 80:1248–1250. [PubMed: 3771931]

European Committee for Medical Ultrasound Safety (ECMUS). ECMUS Radiation stress and its bio-effects. Eur J Ultrasound. 2000; 11:61–64. [PubMed: 10717516]

Elrod SA, Hadimioglu B, Khuri-Yakub BT, Rawson EG, Richley E, Quate CF, Mansour NN, Lundgren TS. Nozzleless droplet formation with focused acoustic beams. J Appl Phys. 1989; 65:3441–3447.

Flecknel, P. Laboratory Animal Anaesthesia. London: Academic Press; 2009.

Frizzell LA, Chen E, Lee C. Effects of pulsed ultrasound on the mouse neonate: hind limb paralysis and lung hemorrhage. Ultrasound Med Biol. 1994; 20:53–63. [PubMed: 8197627]

Frizzell LA, Zachary JF, O'Brien WD Jr. Effect of pulse polarity and energy on ultrasound-induced lung hemorrhage in adult rats. J Acoust Soc Am. 2003; 113:2912–2918. [PubMed: 12765408]

Fu Z, Heldt GP, West JB. Increased fragility of pulmonary capillaries in newborn rabbit. Am J Physiol Lung Cell Mol Physiol. 2003; 284:L703–9. [PubMed: 12676761]

Hartman C, Child SZ, Mayer R, Schenk E, Carstensen EL. Lung damage from exposure to the fields of an electrohydraulic lithotripter. Ultrasound Med Biol. 1990; 16:675–679. [PubMed: 2281556]

Hartman CL, Child SZ, Penney DP, Carstensen EL. Ultrasonic heating of lung tissue. J Acoust Soc Am. 1992; 91:513–516. [PubMed: 1737892]

Holland CK, Deng CX, Apfel RE, Alderman JL, Fernandez LA, Taylor KJ. Direct evidence of cavitation in vivo from diagnostic ultrasound. Ultrasound Med Biol. 1996; 22:917–925. [PubMed: 8923710]

Hopkins SR, Henderson AC, Levin DL, Yamada K, Arai T, Buxton RB, Prisk GK. Vertical gradients in regional lung density and perfusion in the supine human lung: the Slinky effect. J Appl Physiol (1985). 2007; 103:240–248. [PubMed: 17395757]

Jabaraj DJ, Jaafar MS. Theoretical modelling of alveolar resonance mechanism of ultrasound-induced lung haemorrhage. Pol J Med Phys Eng. 2012; 18:59–71.

Jabaraj DJ, Jaafar MS. Theoretical calculation of bending stiffness of alveolar wall. J Membr Biol. 2013a; 246:981–984. [PubMed: 24121628]

Jabaraj DJ, Jaafar MS. Vibration analysis of circular membrane model of alveolar wall in examining ultrasound-induced lung hemorrhage. J Med Ultrasound. 2013b; 21:81–91.

el-Khatib E, Lehnert S. Lung density changes observed in vivo in rat lungs after irradiation: variations among and within individual lungs. Int J Radiat Oncol Biol Phys. 1989; 16:745–754. [PubMed: 2921173]

Kendall MW, Eissmann E. Scanning electron microscopic examination of human pulmonary capillaries using a latex replication method. Anat Rec. 1980; 196:275–83. [PubMed: 6996523]

Kuhn C 3rd, Finke EH. The topography of the pulmonary alveolus: scanning electron microscopy using different fixations. J Ultrastruct Res. 1972; 38:161–173. [PubMed: 4550613]

Levitzky, MG. Pulmonary Physiology. 8. McGraw Hill; New York: 2013.

Lichtenstein DA, Mezière GA, Lagoueyte JF, Biderman P, Goldstein I, Gepner A. A-lines and B-lines: lung ultrasound as a bedside tool for predicting pulmonary artery occlusion pressure in the critically ill. Chest. 2009; 136:1014–1020. [PubMed: 19809049]

Lichtenstein D. Lung ultrasound in the critically ill. Curr Opin Crit Care. 2014; 20:315–322. [PubMed: 24758984]

Maggiorini M, Mélot C, Pierre S, Pfeiffer F, Greve I, Sartori C, Lepori M, Hauser M, Scherrer U, Naeije R. High-altitude pulmonary edema is initially caused by an increase in capillary pressure. Circulation. 2001; 103:2078–2083. [PubMed: 11319198]

Miller DL. A review of the ultrasonic bioeffects of microsonation, gas-body activation, and related cavitation-like phenomena. Ultrasound Med Biol. 1987; 13:443–470. [PubMed: 3310354]

Miller DL. Induction of pulmonary hemorrhage in rats during diagnostic ultrasound. Ultrasound Med Biol. 2012; 38:1476–1482. [PubMed: 22698500]

Miller DL, Suresh MV, Dou C, Yu B, Raghavendran K. Characterization of ultrasound-induced pulmonary capillary hemorrhage in rats. Microvasc Res. 2014; 93:42–45. [PubMed: 24583360]

Miller DL, Dou C, Raghavendran K. Dependence of thresholds for pulmonary capillary hemorrhage on diagnostic ultrasound frequency. Ultrasound Med Biol. 2015a; 41:1640–1650. [PubMed: 25746909]

Miller DL, Dou C, Raghavendran K. Pulmonary capillary hemorrhage induced by fixed-beam pulsed ultrasound. Ultrasound Med Biol. 2015b; 41:2212–2219. [PubMed: 25933710]

Miller DL, Dou C, Raghavendran K. Anesthetic techniques influence the induction of pulmonary capillary hemorrhage during diagnostic ultrasound scanning in rats. J Ultrasound Med. 2015c; 34:289–297. [PubMed: 25614402]

Miller DL, Dong Z, Dou C, Raghavendran K. Influence of Scan Duration on Pulmonary Capillary Hemorrhage Induced by Diagnostic Ultrasound. Ultrasound Med Biol. 2016a; 42:1942–1950. [PubMed: 27117631]

Miller DL, Dou C, Dong Z, Raghavendran K. The influence of dexmedetomidine on ultrasound-induced pulmonary capillary hemorrhage in rats. Ultrasound Med Biol. 2016b; 42:964–970. [PubMed: 26774471]

Nyborg, WL. Physical principles of ultrasound. In: Fry, FJ., editor. Ultrasound its Applications in Medicine and Biology. Vol. Chap 1. Elsevier Scientific Publishing Co; Amsterdam: 1978. p. 1-76.

Nyborg WL. Biological effects of ultrasound: development of safety guidelines. Part I: personal histories. Ultrasound Med Biol. 2000; 26:911–964. [PubMed: 10996695]

Nyborg, WL.; Carson, PL.; Carstensen, EL.; Dunn, F.; Miller, MW.; Miller, DL.; Thompson, HE.; Ziskin, MC. Exposure Criteria for Medical Diagnostic Ultrasound: II. Criteria Based on All Known Mechanisms. (Report No. 140). Bethesda Md: National Council on Radiation Protection and Measurements; 2002.

O'Brien WD Jr, Frizzell LA, Weigel RM, Zachary JF. Ultrasound-induced lung hemorrhage is not caused by inertial cavitation. J Acoust Soc Am. 2000; 108:1290–1297. [PubMed: 11008829]

O'Brien WD Jr, Simpson DG, Frizzell LA, Zachary JF. Superthreshold behavior and threshold estimates of ultrasound-induced lung hemorrhage in adult rats: role of beamwidth. IEEE Trans Ultrason Ferroelectr Freq Control. 2001; 48:1695–1705. [PubMed: 11800133]

O'Brien WD Jr, Kramer JM, Waldrop TG, Frizzell LA, Miller RJ, Blue JP, Zachary JF. Ultrasound-induced lung hemorrhage: role of acoustic boundary conditions at the pleural surface. J Acoust Soc Am. 2002; 111:1102–1109. [PubMed: 11863166]

O'Brien WD Jr, Simpson DG, Frizzell LA, Zachary JF. Threshold estimates and superthreshold behavior of ultrasound-induced lung hemorrhage in adult rats: role of pulse duration. Ultrasound Med Biol. 2003a; 29:1625–1634. [PubMed: 14654157]

O'Brien WD Jr, Simpson DG, Ho MH, Miller RJ, Frizzell LA, Zachary JF. Superthreshold behavior and threshold estimation of ultrasound-induced lung hemorrhage in pigs: role of age dependency. IEEE Trans Ultrason Ferroelectr Freq Control. 2003b; 50:153–169. [PubMed: 12625588]

O'Brien WD Jr, Simpson DG, Frizzell LA, Zachary JF. Effect of contrast agent on the incidence and magnitude of ultrasound-induced lung hemorrhage in rats. Echocardiography. 2004; 21:417–422. [PubMed: 15209720]

Oelze ML, Miller RJ, Blue JP Jr, Zachary JF, O'Brien WD Jr. Impedance measurements of ex vivo rat lung at different volumes of inflation. J Acoust Soc Am. 2003; 114:3384–3393. [PubMed: 14714818]

Oelze ML, Miller RJ, Blue JP Jr, Zachary JF, O'Brien WD Jr. Estimation of the acoustic impedance of lung versus level of inflation for different species and ages of animals. J Acoust Soc Am. 2008; 124:2340–2352. [PubMed: 19062872]

Raeman CH, Child SZ, Carstensen EL. Timing of exposures in ultrasonic hemorrhage of murine lung. Ultrasound Med Biol. 1993; 19:507–512. [PubMed: 8236592]

Raeman CH, Child SZ, Dalecki D, Cox C, Carstensen EL. Exposure-time dependence of the threshold for ultrasonically induced murine lung hemorrhage. Ultrasound Med Biol. 1996; 22:139–141. [PubMed: 8928311]

Raeman CH, Dalecki D, Child SZ, Meltzer RS, Carstensen EL. Albunex does not increase the sensitivity of the lung to pulsed ultrasound. Echocardiography. 1997; 14:553–558. [PubMed: 11174994]

Sarvazyan AP, Rudenko OV, Nyborg WL. Biomedical applications of radiation force of ultrasound: historical roots and physical basis. Ultrasound Med Biol. 2010; 36:1379–1394. [PubMed: 20800165]

Shiina T, Nightingale KR, Palmeri ML, Hall TJ, Bamber JC, Barr RG, Castera L, Choi BI, Chou YH, Cosgrove D, Dietrich CF, Ding H, Amy D, Farrokh A, Ferraioli G, Filice C, Friedrich-Rust M, Nakashima K, Schafer F, Sporea I, Suzuki S, Wilson S, Kudo M. WFUMB guidelines and recommendations for clinical use of ultrasound elastography: Part 1: basic principles and terminology. Ultrasound Med Biol. 2015; 41:1126–1147. [PubMed: 25805059]

Schraufnagel DE, Mehta D, Harshbarger R, Treviranus K, Wang NS. Capillary remodeling in bleomycin-induced pulmonary fibrosis. Am J Pathol. 1986; 125:97–106. [PubMed: 2430459]

Short AC1, Montoya ML, Gebb SA, Presson RG Jr, Wagner WW Jr, Capen RL. Pulmonary capillary diameters and recruitment characteristics in subpleural and interior networks. J Appl Physiol (1985). 1996; 80:1568–1573. [PubMed: 8727541]

Simon JC, Sapozhnikov OA, Khokhlova VA, Wang YN, Crum LA, Bailey MR. Ultrasonic atomization of tissue and its role in tissue fractionation by high intensity focused ultrasound. Phys Med Biol. 2012; 57:8061–8078. [PubMed: 23159812]

Swayne GT, Smaje LH. Dynamic compliance of single perfused frog mesenteric capillaries and rat venules: a filtration coefficient correction. Int J Microcirc Clin Exp. 1989; 8:43–52. [PubMed: 2722410]

Tjan KK, Phillips WRC. On impulsively generated inviscid axisymmetric surface jets, waves and drops. Journal of Fluid Mechanics. 2007; 576:377–403.

Tjan KK, Phillips WRC. On the impulsive generation of drops at the interface of two inviscid fluids. Proc R Soc A. 2008; 464:1125–1140.

Volpicelli G. Lung sonography. J Ultrasound Med. 2013; 32:165–171. [PubMed: 23269722]

Wang, TC.; Lee, CP. Radiation pressure and acoustic levitation. In: Hamilton, MF.; Blackstock, DT., editors. Nonlinear Acoustics. Vol. Chap 6. Academic Press; New York, NY: 1998. p. 177-205.

West JB. Invited review: pulmonary capillary stress failure. J Appl Physiol (1985). 2000; 89:2483–2489. [PubMed: 11090605]

West JB. Fragility of pulmonary capillaries. J Appl Physiol (1985). 2013; 115:1–15. [PubMed: 23640584]

West JB, Mathieu-Costello O. High altitude pulmonary edema is caused by stress failure of pulmonary capillaries. Int J Sports Med. 1992a; 13(Suppl 1):S54–S58. [PubMed: 1483792]

West JB, Mathieu-Costello O. Strength of the pulmonary blood-gas barrier. Respir Physiol. 1992b; 88:141–148. [PubMed: 1626133]

West JB, Mathieu-Costello O. Structure, strength, failure, and remodeling of the pulmonary blood-gas barrier. Annu Rev Physiol. 1999; 61:543–572. [PubMed: 10099701]

West JB, Tsukimoto K, Mathieu-Costello O, Prediletto R. Stress failure in pulmonary capillaries. J Appl Physiol (1985). 1991; 70:1731–1742. [PubMed: 2055852]

Zachary JF, Sempsrott JM, Frizzell LA, Simpson DG, O'Brien WD Jr. Superthreshold behavior and threshold estimation of ultrasound-induced lung hemorrhage in adult mice and rats. IEEE Trans Ultrason Ferroelectr Freq Control. 2001; 48:581–592. [PubMed: 11370372]

Zachary JF, Blue JP Jr, Miller RJ, Ricconi BJ, Eden JG, O'Brien WD Jr. Lesions of ultrasound-induced lung hemorrhage are not consistent with thermal injury. Ultrasound Med Biol. 2006; 32:1763–1770. [PubMed: 17112962]

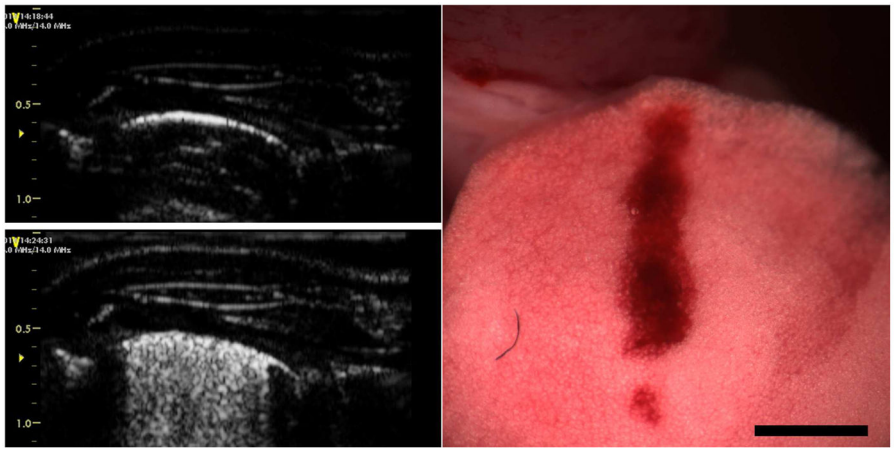

Fig. 1.

Diagnostic ultrasound images at 12.0 MHz before (left, top) and after (left, bottom) scanning with the resulting PCH shown on the right (scale bar: 2 mm). The ultrasound images show a portion of the rat thorax with the bright lung surface images displayed at about 5 mm from the skin surface. At the end of scanning, comet tail artifacts extended across nearly the entire lung surface image, which corresponded to the PCH seen on the lung surface. Reproduced from Miller et al. (2015a).

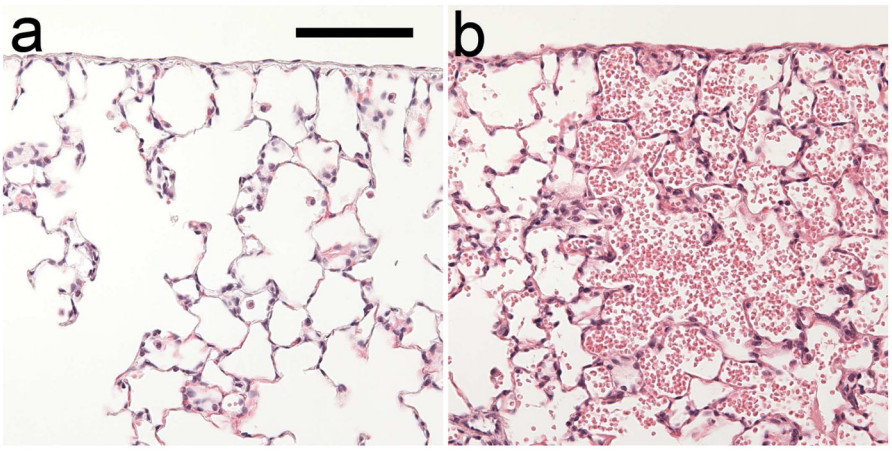

Fig. 2.

Histology of fixed lung samples with hematoxylin and eosin staining. Outside the PCH volume (a), the normal pulmonary structure is visceral pleura and thin alveolar septa with connected gas channels. Within the PCH volume (b), many alveoli contain erythrocytes from the hemorrhage but no apparent hemorrhage into the interstitium (alveolar septa). Photomicrographs were from the same slide shown in Fig. 4 of Miller (2012). Scale bar: 0.1mm.

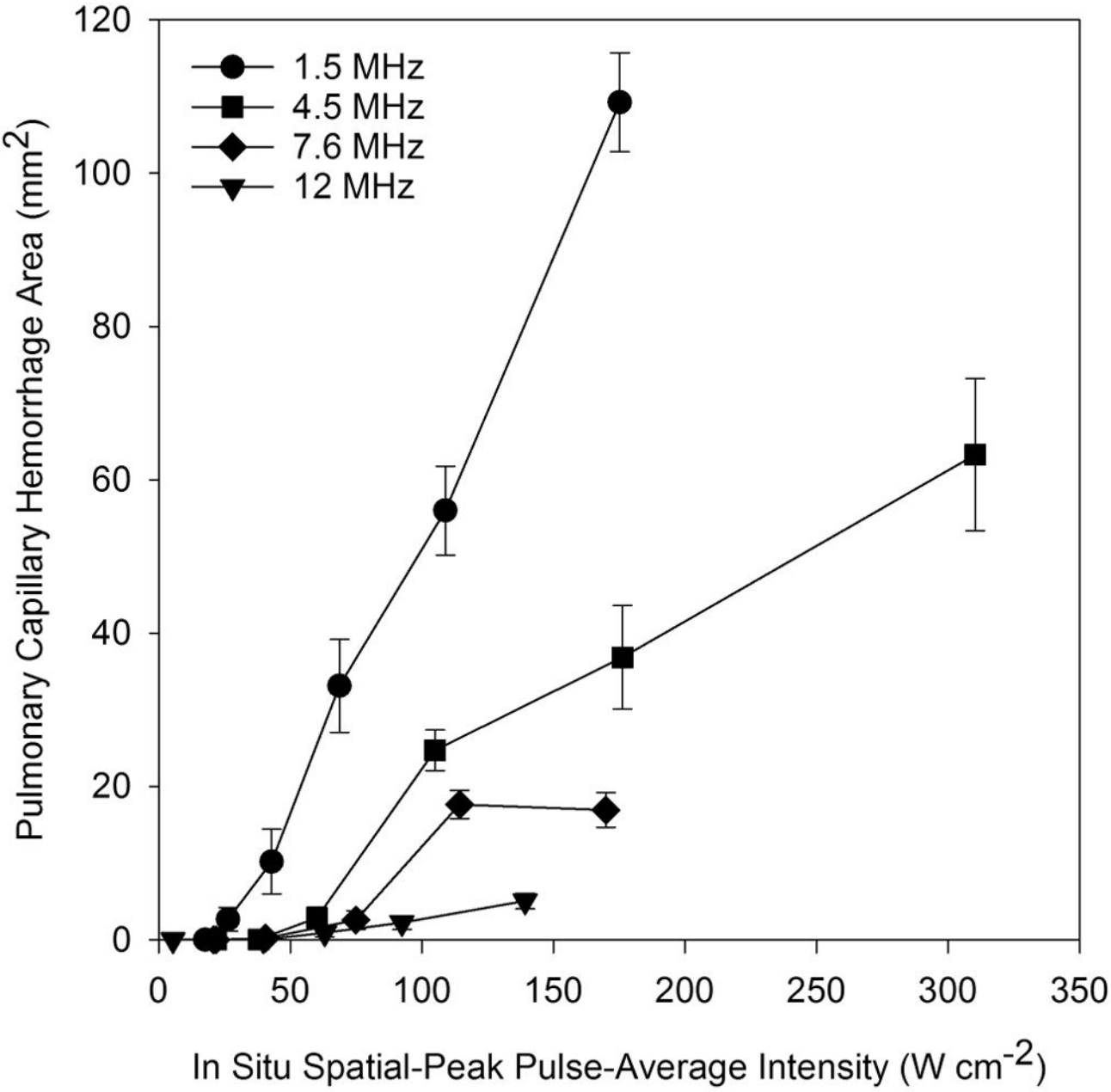

Fig. 3.

PCH area replotted against pulse average intensity response from Fig. 8 of Miller et al. (2015a). The PCH for each frequency of diagnostic ultrasound increases above an apparent threshold. The magnitude of PCH decreases for increasing ultrasound frequency, but the thresholds are nearly constant with frequency (see Table 1).

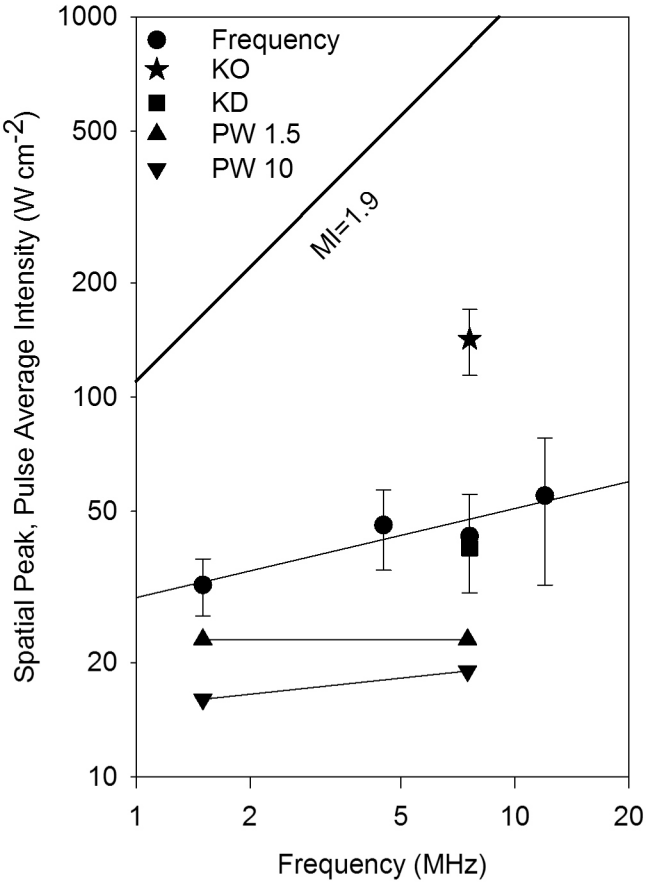

Fig. 4.

Pulse average intensity thresholds for rats plotted against frequency. The log-log plot shows equivalent intensities for the guideline upper limit of the Mechanical Index (MI=1.9) as the diagonal line (proportional to frequency). The frequency data were from Miller et al. (2015a), the threshold for ketamine only anesthesia (KO) was from Miller et al. (2015c), and the threshold for ketamine with dexmedetomidine (KD) was from Miller et al. (2016b), with error bars associated with determination of threshold by linear regression of the dose-response data. The pulse wave thresholds for ~1.5 μs (PW 1.5) and ~10 μs (PW 10) were from Miller et al. (2015b).

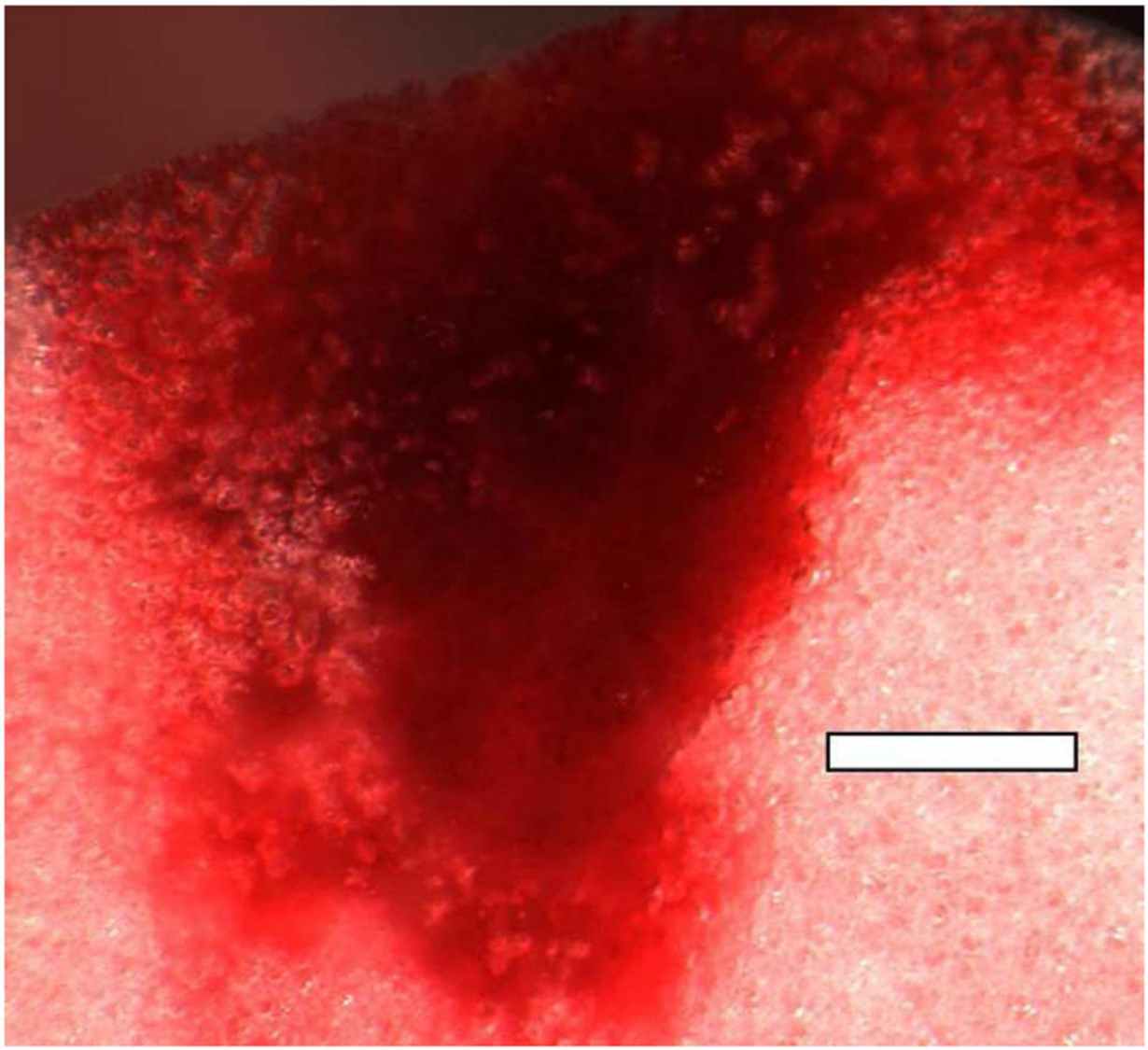

Fig. 5.

A PCH area induced by scanning at an on screen MI=0.9 at 7.6 MHz (image from the study reported in Miller et al. (2014)). The alveolar gas has greatly diminished in the PCH volume, but residual bodies of gas remain as bubbles of about 100 μm diameter or less. Scale Bar: 1 mm.

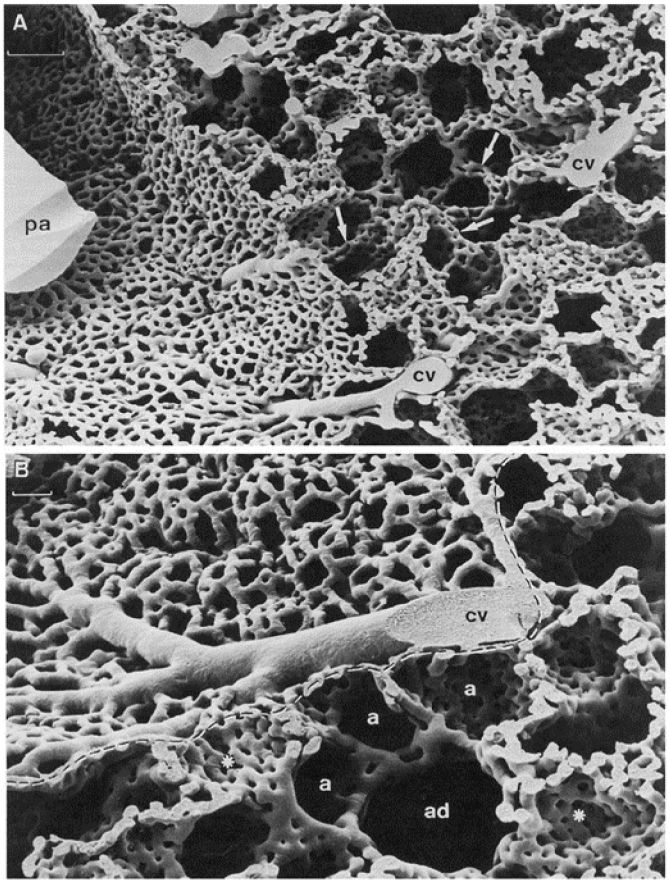

Fig. 6.

Scanning electron microscope images of pulmonary capillary morphology produced using the cast and corrosion method. A. a vascular cast of 139 day old rat lung with a 50 μm scale marker: collecting vein (cv), pulmonary artery branch (pa). Alveolar entry rings are noted by arrows. B. vascular cast of a 44 day old rat lung with 20 μm scale marker: alveoli (a), alveolar duct (ad). The dense meshwork of capillaries allow the alveolar morphology to be recognized even after tissue removal, and illustrate the complex structures with which ultrasound pulses interact. Reproduced with permission from Caduff et al. (1986).

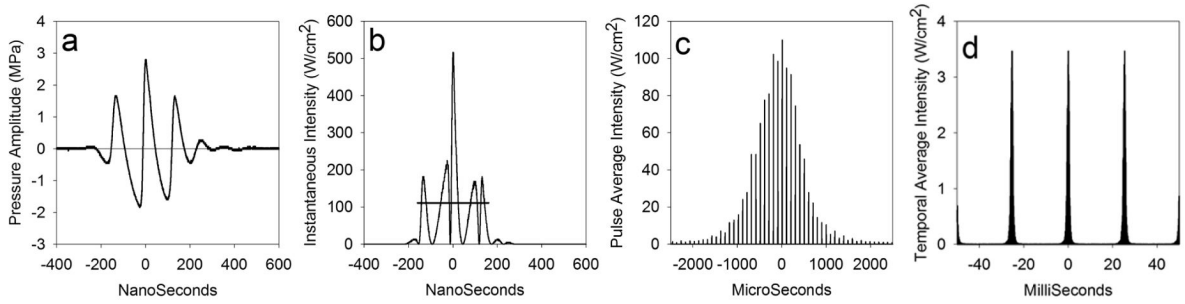

Fig. 7.

An illustration of the time scales involved in diagnostic ultrasound scanning at 7.6 MHz with MI=0.9 and derated for the chest wall attenuation as in Miller (2012): (a) derated pulse pressure waveform (from the hydrophone), and (b) the instantaneous intensity used to calculate the pulse average intensity and pulse duration, which are indicated by the horizontal line (111 Wcm^{-2} and 320 ns) plotted in ns; (c) the pulse average intensity of pulses arriving at 10 kHz PRF (each 100 μs) as the beam scans past the hydrophone plotted in μs; (d) the temporal average intensity (pulse average intensity times the duty cycle of 0.032) of a series of scans at 39 frames per second plotted in ms. The PRF temporal average intensity is further reduced by the scan duty cycle of about 0.04, giving and overall spatial peak, temporal average intensity of about 0.07 Wcm^{-2}. Although the magnitudes of the instantaneous parameters during the pulses are substantial, which have a potential for cavitation or other nonthermal mechanisms, the overall temporal average energy delivery is very low, which yields insignificant potential for heating.

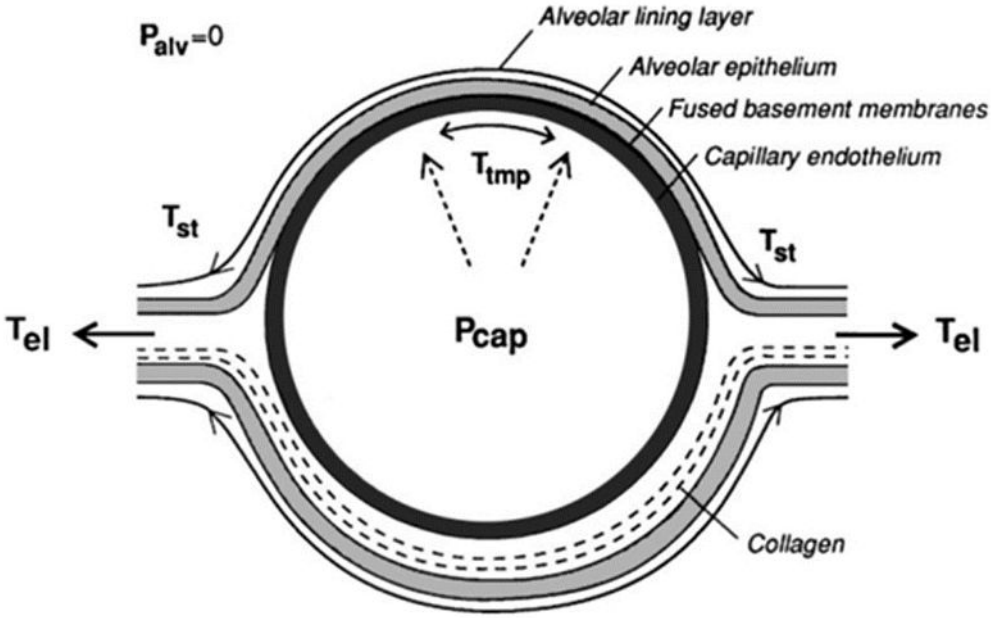

Fig. 8.

A diagram of the structures and stresses for a pulmonary capillary within an alveolar septa. There are forces produced by surface tension (T_{st}), longitudinal stress (T_{el}) and transmural pressure difference (T_{tmp}) between P_{alv} of the alveolar gas and P_{cap} within the capillary (above atmospheric pressure). Excess capillary pressure can cause the blood-air barrier to fail at the very thin interface leading to PCH. Reprinted with permission from West (2000).

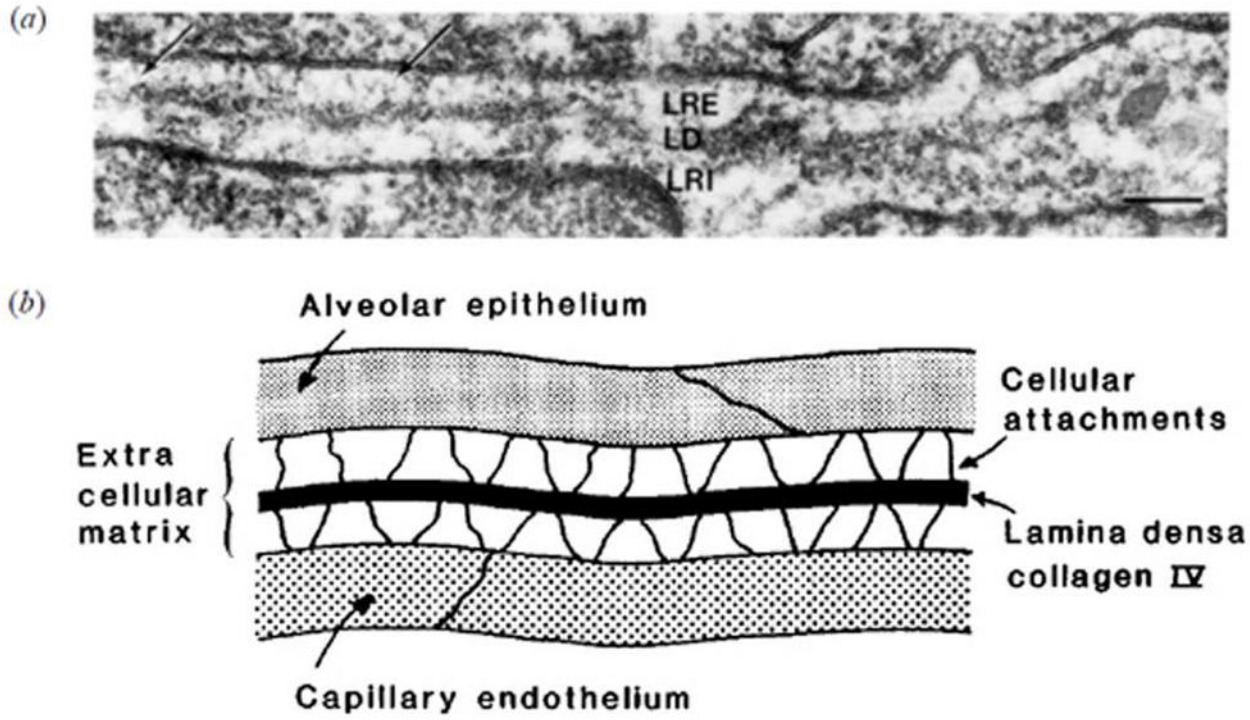

Fig. 9.

An electron microscope image (scale bar 0.1 μm) (a) and diagram illustrating the structure of the thin part of the blood air barrier (b). The extracellular matrix between the epithelium and endothelium consists of a lamina rara externa (LRE), laminar rara interna (LRI) and the very thin lamina densa (LD) providing strength by the collagen IV layer about 50 nm thick. Reprinted with permission from West (2000).

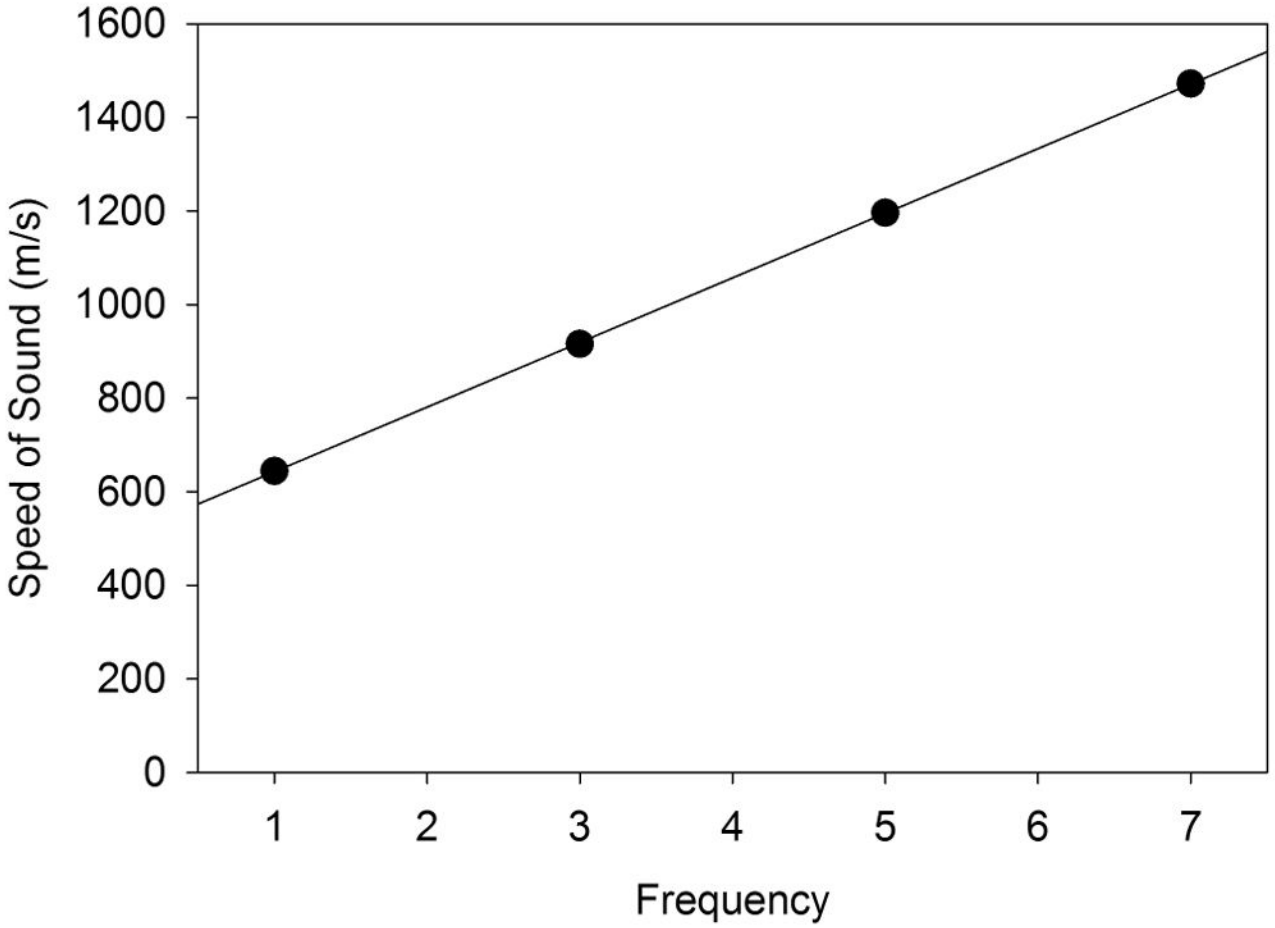

Fig. 10.

The bulk speed of sound in lung is dependent on the lung inflation and the ultrasound frequency (Dunn, 1986). The data were for a bulk mass density of 400 kg/m^3, corresponding to approximately normal inflation of lung.

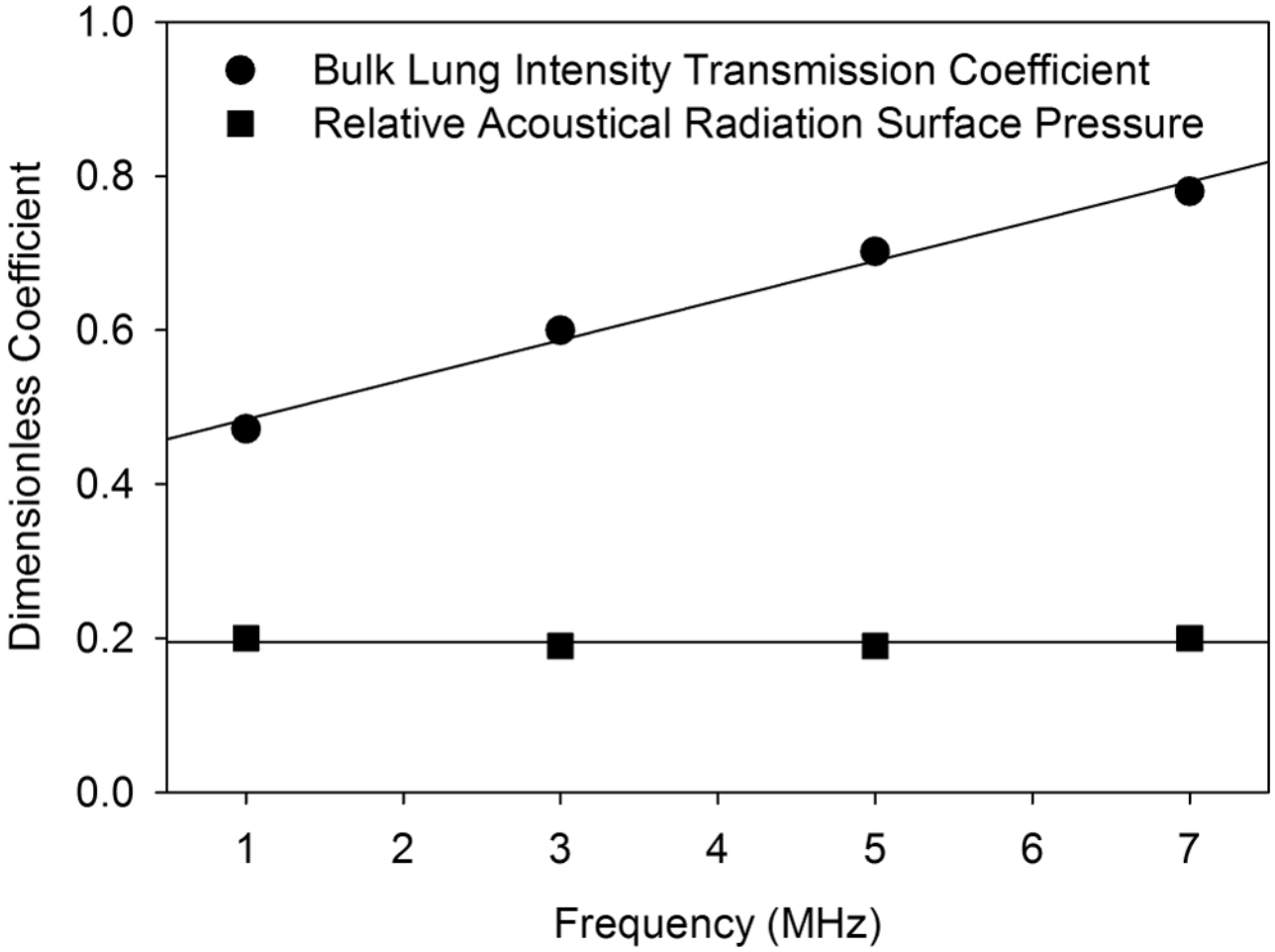

Fig. 11.

The intensity transmission coefficient, calculated from bulk data for lung of speed of sound (Fig. 10) and density 400 kg/m^3 (Dunn, 1986), increases with frequency. The ratio of $\mathbf{P_{SRb}}$ to $\mathbf{P_{SRa}}$, calculated from Eqn. 2, is reduced owing to the intensity transmission (reduced reflection) to about 0.2 for the assumed conditions.

Table 1

Recent results for in situ PCH thresholds (determined as exposure-response intercepts) given as PRPA and $\mathbf{I_{sppa}}$ with the $\mathbf{P_{RSa}}$ calculated from Eq. 1.

Condition	Frequency MHz	Pulse Dur μs	PRPA MPa	I_{sppa} Wcm^{-2}	P_{RSa} Pa	P_{RSa} mmHg	Reference
Pulse wave	1.5	1.7	0.76	23	311	2.3	2015b
Pulse wave	1.5	10.3	0.65	16	214	1.5	2015b
Pulse wave	7.5	0.3	0.77	23	367	2.7	2015b
Pulse wave	7.5	1.5	0.76	23	300	2.2	2015b
Pulse wave	7.5	10.3	0.70	19	247	1.8	2015b
B mode	1.5	1.5	1.0	32	426	3.2	2015a
B mode	4.5	0.3	1.2	46	612	4.6	2015a
B mode	7.6	0.25	1.0	43	572	4.3	2015a
B mode*	7.6	0.25	1.9	142	1889	13.9	2015c
B mode	12.0	0.16	1.2	55	732	5.4	2015a

Anesthesia was with ketamine plus xylazine, except for one condition with ketamine only (*). References are Miller et al. (2015a, 2015b, 2015c). Abbreviations: Duration (Dur), radiation surface pressure (**PRS**a).

Table 2

Estimates from Eq. 2 for the reduction of acoustical radiation pressure at the surface for the bulk model P_{SRb} relative to a tissue-air interface P_{RSa} for transmission of ultrasound into the lung with a lung density of ρ_{lung} = 400 kgm^{-3} and speeds of sound c_{lung} from values given by Dunn (1986). The density and speed of sound for the tissue side of the blood-air barrier were taken to be ρ_{tis} = 1050 kg m^{-3} and c_{tis} = 1550 m s^{-1}, respectively. The intensity transmission coefficient (ITC) is also given to indicate the potential energy penetrating into the interior of the lung.

Frequency MHz	c_{lung} m s^{-1}	ρ_{lung} c_{lung} krayl	c_{tis}/c_{lung}	Z	P_{SRb}/P_{RSa}	ITC
1.0	644	258	2.4	6.3	0.20	0.47
1.5	712	285	2.2	5.7	0.19	0.51
3.0	916	366	1.7	4.4	0.19	0.60
4.5	1126	450	1.4	3.6	0.19	0.68
5.0	1196	478	1.3	3.4	0.19	0.70
7.0	1472	589	1.1	2.8	0.20	0.78
7.5	1541	616	1.0	2.6	0.20	0.80